

Linköping University Post Print

Cross-field ion transport during high power impulse magnetron sputtering

Daniel Lundin, Petter Larsson, Erik Wallin, Martina Lattemann,
Nils Brenning and Ulf Helmersson

N.B.: When citing this work, cite the original article.

Original Publication:

Daniel Lundin, Petter Larsson, Erik Wallin, Martina Lattemann, Nils Brenning and Ulf Helmersson, Cross-field ion transport during high power impulse magnetron sputtering, 2008, Plasma Sources Science and Technology, (17), 035021.

<http://dx.doi.org/10.1088/0963-0252/17/3/035021>

Copyright: Iop Publishing

<http://www.iop.org/>

Postprint available at: Linköping University Electronic Press

<http://urn.kb.se/resolve?urn=urn:nbn:se:liu:diva-13209>

Cross-field ion transport during high power impulse magnetron sputtering

Daniel Lundin¹, Petter Larsson¹, Erik Wallin¹, Martina Lattemann^{1, 2}, Nils Brenning³ and Ulf Helmersson¹

¹ Plasma & Coatings Physics Division, IFM-Materials Physics, Linköping University, SE-581 83 Linköping, Sweden

² Joint Research Laboratory Nanomaterials, TU Darmstadt and Forschungszentrum Karlsruhe GmbH, Petersenstraße 23, D-64287 Darmstadt, Germany

³ Division of Space and Plasma Physics, School of Electrical Engineering, Royal Institute of Technology, SE-100 44 Stockholm, Sweden

E-mail: danlu@ifm.liu.se

Abstract

In this study, the effect on thin film growth due to an anomalous electron transport, found in high power impulse magnetron sputtering (HiPIMS) has been investigated for the case of a planar circular magnetron. An important consequence of this type of transport is that it affects the way ions are being transported in the plasma. It was found that a significant fraction of ions are transported radially outwards in the vicinity of the cathode, across the magnetic field lines, leading to increased deposition rates directly at the side of the cathode (perpendicular to the target surface). Furthermore, this mass transport parallel to the target surface leads to that the fraction of sputtered material reaching a substrate placed directly in front of the target is substantially lower in HiPIMS compared to conventional direct current magnetron sputtering (dcMS). This would help to explain the lower deposition rates generally observed for HiPIMS compared to dcMS. Moreover, time-averaged mass spectrometry measurements of the energy distribution of the cross-field transported ions were carried out. The measured distributions show a direction-dependent high-energy tail, in agreement with predictions of the anomalous transport mechanism.

Introduction

In high power impulse magnetron sputtering (HiPIMS), introduced in the 90ies [1, 2], plasma densities up to 10^{19} m^{-3} can be reached close to the target race track [3, 4], which should be

compared to 10^{15} - 10^{16} m⁻³ for direct current magnetron sputtering (dcMS) [5]. Due to the plasma conditions in this pulsed plasma, a high degree of ionization of the deposition flux as well as an inherently high energy of the depositing species are obtained, while still keeping the average power at a reasonable level [6]. Therefore, and due to the fact that it is easily applied in a standard magnetron sputtering equipment, HiPIMS is a promising addition to commonly used ionized physical vapor deposition (IPVD) techniques for applications such as filling of narrow trenches in integrated circuits [2]. Moreover, the use of HiPIMS has resulted in improved film quality [7], especially at low temperatures, and controlled film growth through the use of substrate bias to control the momentum transfer from ion bombardment.

The deposition rate in the HiPIMS discharge is commonly found to be lower than that obtained for dcMS at the same average power. Christie [8] suggested self-sputtering due to back-attraction of metal ions to the target as a reason for this. A correlation between the deposition rate and the self-sputtering yield has also been observed experimentally [6,9]. Konstantinidis *et al.* [10] pointed out the importance of the plasma conductivity, while Bugaev *et al.* [11] and Bohlmark *et al.* [12] showed that the magnetic arrangement affected the deposition rate. It is important to keep in mind that the spatial distribution of the deposition flux is in general not necessarily the same for dcMS and HiPIMS, since the ionized deposition species will be affected by fields and energy fluxes in the plasma in a different way than for neutrals. Bohlmark *et al.* demonstrated this by adding an adjustable magnetic field to focus the deposition flux, and thereby increase the deposition rate on a sample position in front of the target while decreasing the amount of deposited material on substrates placed on the side of the magnetron, perpendicular to the target surface [12]. Another aspect is the non-linear dependence of the sputter yield as function of the applied voltage, which was recently discussed by Emmerlich *et al.* [13], pointing out that it is unphysical to compare HiPIMS and dcMS deposition rates for the same average power. In conclusion, it is most likely a combination of the factors mentioned above, and possibly others, that affect the deposition rate, which highlights the importance of looking into the particle transport.

Factors that may affect the spatial distribution of the deposition flux include azimuthal currents (such as the Hall current) generated close to the target surface, which can couple energy between electrons and ions, resulting in modified transport properties. Measurements by Bohlmark *et al.* [14] showed anomalous fast electron transport in HiPIMS discharges, which has been further investigated by Lundin *et al.* [15] and is understood as follows: In HiPIMS, large discharge currents in the plasma between the sputtering cathode and the anode (often the chamber walls and the ground shield of the magnetron) are generated. Furthermore, large azimuthal currents, \mathbf{J}_ϕ , circulating in the magnetic field trap close to the magnetron, arise due to the presence of the magnetic field through a combination of diamagnetic and $\mathbf{E} \times \mathbf{B}$ drifts of electrons. The currents correspond to azimuthal ion-electron drift velocities ranging from about $1.3 \times 10^4 \text{ m s}^{-1}$ at $z = 0.01 \text{ m}$ (above the target surface) to $5 \times 10^4 \text{ m s}^{-1}$ at $z = 0.04 \text{ m}$, which is well above both the typical speed of 5 eV sputtered particles ($< 5 \times 10^3 \text{ m s}^{-1}$) and the ion acoustic speed of Ar^+ ions ($\sim 2 \times 10^3 \text{ m s}^{-1}$). The current is therefore two-stream (cross- \mathbf{B}) unstable according to linear theory [16] and drives the modified two-stream instability (MTSI), the lower hybrid drift instability, or a mixture of both [17]. The underlying mechanisms within this class of instabilities are known both from simulations of critical ion velocities in plasmas and plasma gun transport mechanisms [18, 19], and from measurements in a plasma gun [19] operated in the same plasma parameter regime as reported in the present work. The dominating frequency of the instability is in the lower hybrid range [20], and the variations in density and electric fields (waves) are correlated. Due to this correlation, the waves give a net force $\mathbf{F}_{ei} = \langle e \mathbf{E}_{w,\phi} n_e \rangle$ from electrons to ions, directed along the azimuthal current density, \mathbf{J}_ϕ (see Figure 1a). Here $\mathbf{E}_{w,\phi}$ is the azimuthal electric field of the waves. Therefore a cross-field ion mass transport directed tangentially outwards in the HiPIMS discharge is expected.

In this article the effect of a modified ion transport on thin film growth by changes in flux direction as well as energies is investigated. The expected cross-field ion transport is analyzed by measuring the deposition rate at several positions perpendicular to the target

surface. Furthermore, time-averaged ion energy distribution measurements have been undertaken to measure the energies of the cross-field transported ions in order to verify the expected tangential acceleration.

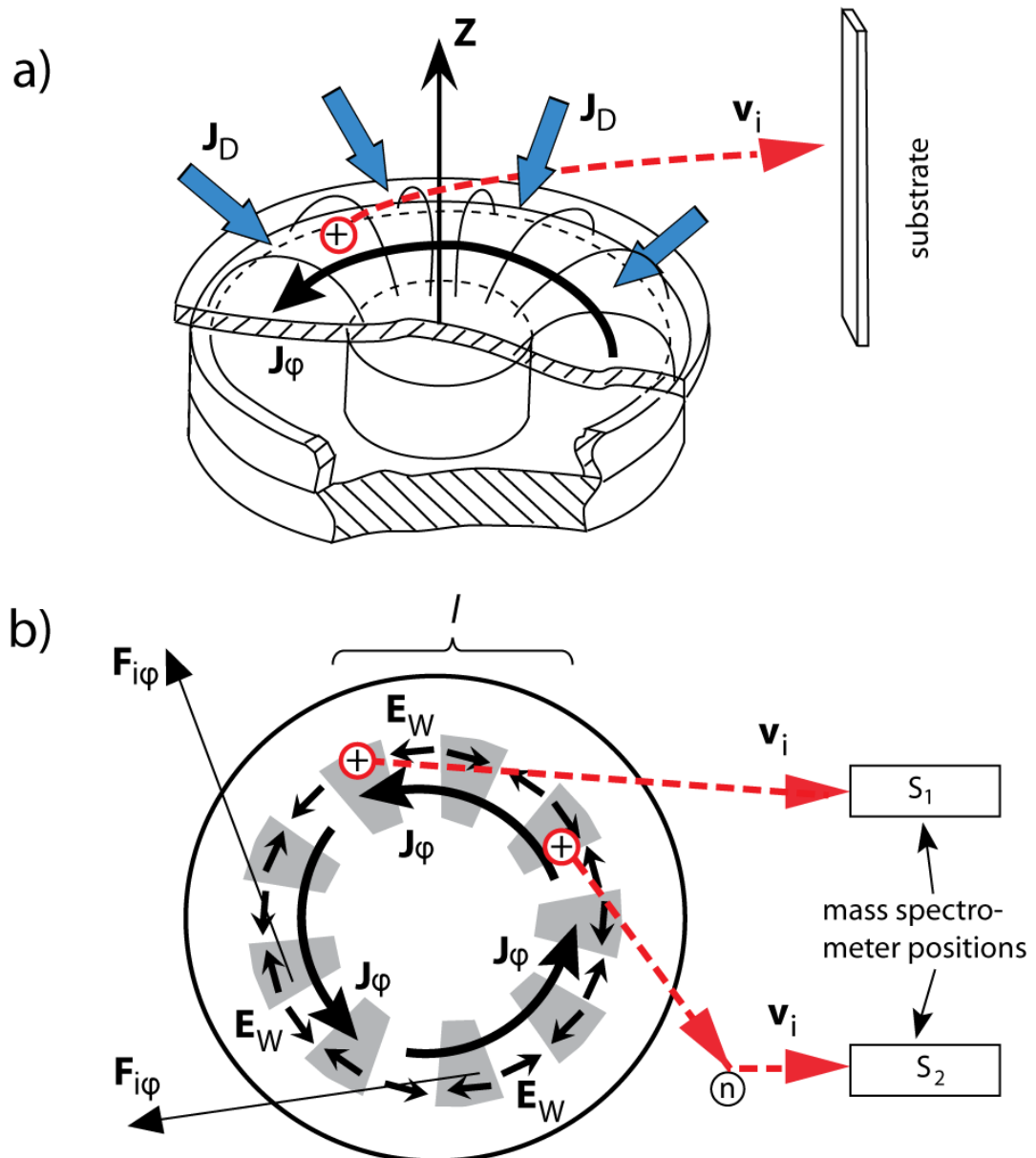


Figure 1. The current system in a magnetron, and how it is related to the sideways ion deflection.
 a) The azimuthal current J_ϕ and the discharge current J_D are perpendicular to B . Both exert forces on the ions. b) Illustration of the microscopic nature of the force from J_ϕ . The dashed arrows show the deflection of ions sideways towards the substrate where the enhanced deposition rate is measured. $F_{i\phi}$ is the ion force, v_i is the ion velocity, and n symbolizing the neutral background gas. E_w is the oscillating electric wave field (oscillations are indicated by the grey and white stripes) found in the anomalous transport [15] and l is the length scale which is approximately 0.05 m.

Experimental details

Two different deposition systems were used in the experiments. The first setup (used for depositing films) consisted of a standard planar circular $\Phi = 0.15$ m magnetron equipped with a Ti (99.9 %) or Cr (99.9 %) target in a cylindrical vacuum chamber (height 0.70 m, diameter 0.44 m) pumped with a turbo-molecular pump to a background pressure of about 1.5×10^{-4} Pa, after which 0.4 Pa of an inert gas (Ar with a minimum purity of 99.9997 %) was let into the chamber. High-voltage pulses were applied between the cathode (target) and the chamber walls using a HiPIMS power supply (Sinex 2, Chemfilt Ionputtering AB). In this work 90 μ s pulses of approximately 700 V were used at a repetition frequency of 300 Hz, resulting in a peak current of about 170 A, a pulse energy of 2.2 J/pulse and an average power of approximately 0.66 kW. Si substrates were placed on two substrate holders (see Figure 2): (A) parallel to the target surface at a distance of $z = 0.100$ m and (B) perpendicular to the target surface at a radial distance of $\rho = 0.096$ m from the target center. On holder (A) a reference substrate was placed below the target race track at $z = 0.100$ m, $\rho = 0.030$ m. Several positions were investigated on substrate holder (B) at a distance in z varied between 0.025-0.120 m. For reference measurements, two direct current (dc) power supplies (TCR 600 V, 3 A, Electronic Measurements Inc.) were used. They were connected in series to the magnetron providing the same average power as for the HiPIMS case. The deposition rates were deduced based on film thickness measurements in a scanning electron microscope.

The second deposition system was used for time-averaged ion energy distribution measurements. Here, a planar circular $\Phi = 0.076$ m magnetron (Gencoa Ltd) equipped with a Ti (99.9 %) target was mounted to a cylindrical vacuum chamber (height 0.30 m, diameter 0.42 m) pumped with a turbo-molecular pump to a background pressure of about 1.5×10^{-4} Pa, after which Ar, with a minimum purity of 99.9997 %, was let into the chamber. The position of the magnetron was adjustable in the z direction (see Figure 3). Unipolar voltage pulses were applied to the magnetron by a pulsing unit (SPIK 1000A, Melec GmbH) charged by a dc power supply (Pinnacle, Advanced Energy) delivering constant voltage pulses of controlled

length. 70 μs pulses of approximately 500 V and 270 A were used, resulting in about 1.1 J/pulse with an average power of about 100 W. For conventional dc reference measurements, a dc power supply (MDX 1K, Advanced Energy) was connected to the magnetron.

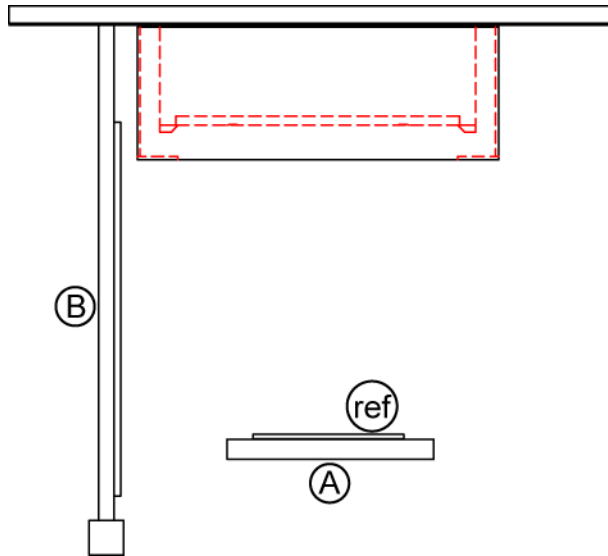


Figure 2. A schematic cross-section of the magnetron and the lid of the deposition chamber with substrate holders (A) and (B) mounted. The location for the reference measurements is also marked (ref).

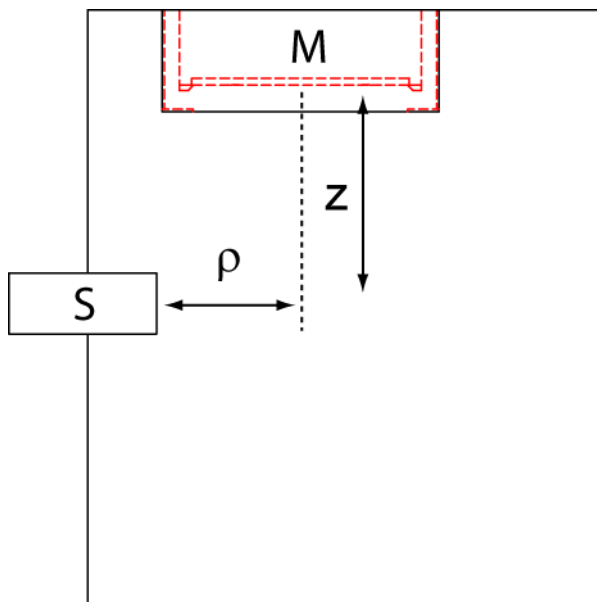


Figure 3. A schematic cross-section of the magnetron (M) and mass spectrometer (S) of the system used for measuring ion energy distributions. The z position of the magnetron was adjusted between 0 and 0.05 m while ρ was kept at 0.05 m.

For the ion energy distribution measurements, an energy resolving mass spectrometer (PSM003, Hiden Analytical) was used. It was inserted into the chamber with the sampling orifice radially positioned about 0.05 m from the center axis of the magnetron (see Figure 3). The magnetron was mounted in the radial direction about 0.025 m off-axis, so that the race track was in line with the orifice of the mass spectrometer. For most measurements (if not otherwise stated), the orifice was placed in position S_1 according to Figure 1b. Due to the adjustable position of the magnetron, the distance between the orifice and the target surface could be varied in z from about 0 – 0.05 m, as can be seen in Figure 3. This means that ion energy distributions for different z positions could be investigated, which corresponds to inserting a mass spectrometer at the different positions displayed in Figure 2. The mass spectrometer was capable of measuring ion energies up to 100 eV with a resolution of 0.05 eV and masses up to 300 amu, with a resolution of 0.01 amu (for more specific details on the mass spectrometer see reference [21]). The energy distributions presented here were all collected under constant spectrometer settings. It has to be noted that the acceptance angle of the mass spectrometer is dependent on the ion energy, meaning that the acceptance angle gets smaller with increasing ion energy. Thus, it is less likely to measure all the incoming high-energy ions compared to the low-energy ions. No exact values are available from the manufacturer for this specific mass spectrometer, but can be estimated to be similar as those given for the EQP mass spectrometer produced by the same manufacturer (see Table 1) [22], using the same extraction optics (the only difference is the use of different energy filters).

Energy [eV]	Acceptance angle [deg]
1	20
5	10
10	9
30	3
80	< 2

Table 1. Acceptance angle for different ion energies based on calculations on the EQP mass spectrometer by Hiden Analytical.

Results

The deposition rate perpendicular to the target surface for HiPIMS and dcMS was measured for both Ti and Cr and normalized to the deposition rate parallel to the target (at point (ref), see Figure 2). The normalized deposition rates at different distances from the target are plotted in Figure 4. From this figure it is clear that the deposition rate in both HiPIMS and dcMS is the largest at the reference position, but that a large amount of material is also transported sideways. It is seen that the maximum side-deposition rate is reached around $z = 0.055$ m where the deposition rate of Ti is approximately 80 % and 70 % for HiPIMS and dcMS respectively, compared to the deposition rate for the reference position. Corresponding values for Cr is 50 % and 40 %. An average over the whole measured area gives about 10 % and 25 % higher HiPIMS deposition rate for Ti and Cr, respectively. Worth noticing is that the deposition rate for HiPIMS was about 21 % (for Ti) and 40 % (for Cr) of the dcMS rates at the reference position at equal average powers. This lower deposition rate for HiPIMS is in line with what has previously been reported [9].

Investigations of ion energies of the ions deflected sideways from the magnetron have been carried out for Ti^+ measured in the HiPIMS plasma at different z distances from the target race track. The results are displayed in Figure 5. In all cases there is a clear ion energy peak of about 1.5 eV followed by a high-energy tail that can be traced up to around 80, 50, 32 and 23 eV for $z = 0.00, 0.01, 0.03, 0.05$ m away from the target race track. The low-energy peak is related to thermalized ions accelerated by the potential drop between the plasma and

the grounded spectrometer. A high-energy tail is also found for dcMS but to a much lesser extent as seen in Figure 6. Another feature is also visible here: in the case of the HiPIMS distribution there is clearly a dip in the energy spectrum around 5 eV followed by a second peak around 10-15 eV, which is not present in the dcMS measurement.

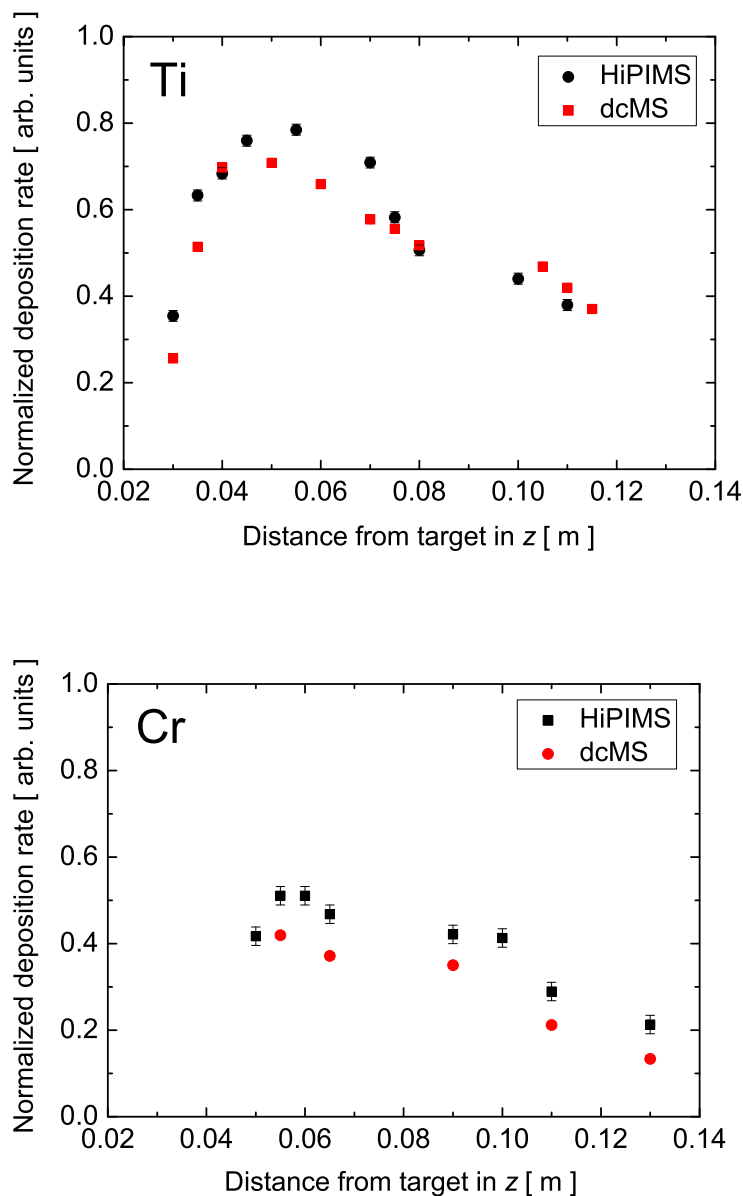


Figure 4. Normalized deposition rates for different substrate positions investigated for Ti and Cr. The films were deposited with dcMS or HiPIMS. All values were normalized with respect to the measured deposition rate (in each experiment) for the substrate placed parallel to the target surface. In most cases the error bars are on the size of the plotted measuring point.

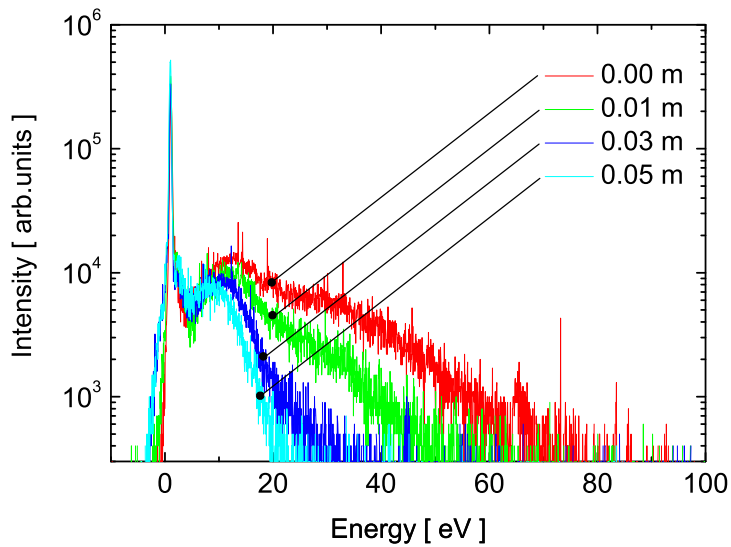


Figure 5. Ti^+ ion energies at 0.53 Pa using 500 V HiPIMS pulses for different distances in z . The average ion energy is found to be around 18 eV when measuring at $z = 0.00$ m.

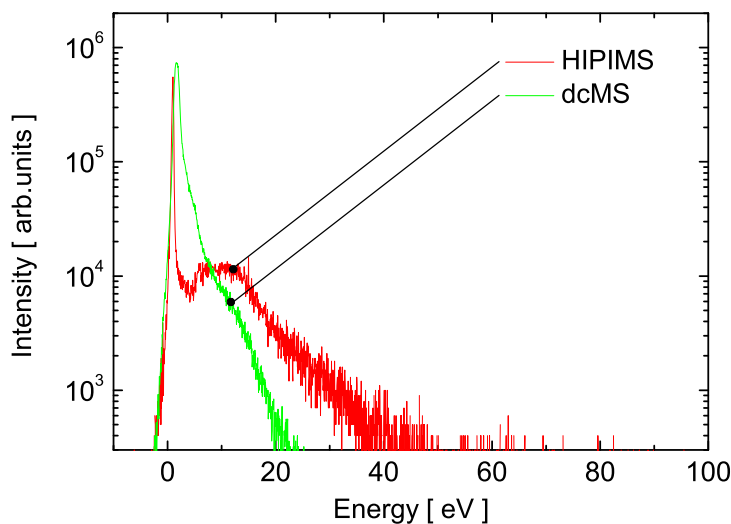


Figure 6. Comparison between Ti^+ ion energies from HiPIMS and dcMS measured at 0.80 Pa and $z = 0.01$ m using equal average power. Note that the displayed intensities are in arbitrary units, and that no correlation between the different abundances of Ti^+ can be made based on this measurement only. Furthermore, the distributions have been normalized to fit into one single plot.

The ion energy distribution was also measured with the spectrometer in two different positions S_1 and S_2 as illustrated in Figure 1b. The result of these measurements (Figure 7)

shows significant higher intensity of the high-energy tail for the measurement in position S_1 . In this position the spectrometer is facing into the race track region where the current is moving away from the spectrometer. This is also the position used for measuring the data presented in Figure 5 and Figure 6.

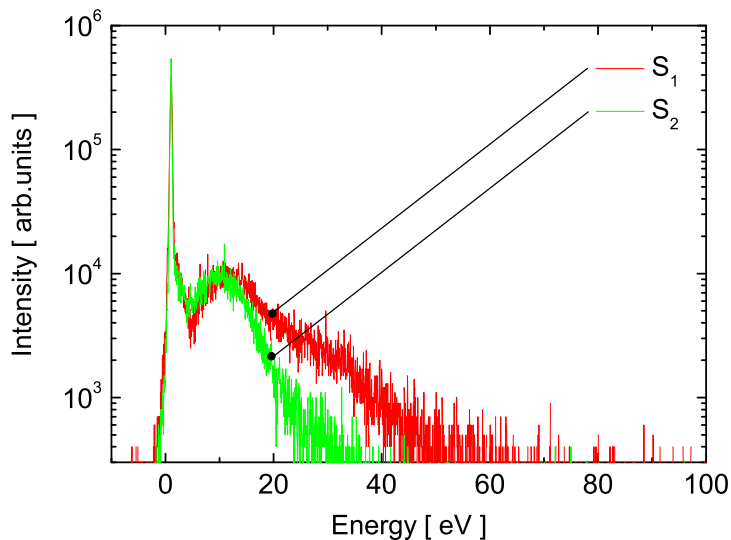


Figure 7. Comparison between Ti^+ ion energies from two different sides of the HiPIMS race track, S_1 and S_2 as indicated in Figure 1b. The measurements were carried out at 0.80 Pa and $z = 0.01$ m using 500 V discharge pulses.

Discussion

The results above show that a substantial amount of sputtered material is being transported sideways in both HiPIMS and dcMS. A significantly larger fraction is ending up on the sides for HiPIMS as compared to dcMS, a conclusion we have drawn after estimating the deposition rate through measurements of the thickness of the coating. This way of estimating the deposition rate suffers from the fact that the film density may be different in the different cases. However, films grown using HiPIMS are likely to be denser due to the energetic bombardment [23], especially for substrate positions where the deposition material is arriving non-perpendicular to the growth surface [7] as in the side deposition case in the present

experiment. It is therefore concluded that it is possible that the difference between the HiPIMS and the dcMS side deposition rates are underestimated in our case.

It is clear from the measurements presented here that a considerable amount of deposition material is captured on the side walls of the deposition vessel, and particularly so in the case of HiPIMS. With the design of the present experiment it is difficult to use the measurements to estimate how much this increased side-transport is contributing to the observed lower HiPIMS deposition rate observed on positions facing the target. However, it cannot be excluded that it is an important factor, especially when considering that the capture surface of the side-wall is considerably larger (approximately 6.5 times) than the surface facing the target in the used experimental set-up.

From the discussion above it is concluded that sputtered material in the HiPIMS mode is deflected sideways, away from the z axis and towards the walls to a larger extent than for dcMS. An increased deflection by collisions with gas neutrals is discarded because the gas background is expected to be strongly reduced during the HiPIMS pulse [24] and that the sideways deflection mechanism gives the metal ions an increased energy (around 20 eV on average). Among electrical forces that could explain the deflection to the sides, an ambipolar diffusion field is unlikely because the electrons are well magnetized but not the ions; an ambipolar electric field with the required direction towards the walls would arise only if the electrons escaped more easily than the ions. Acceleration to the side walls due to the high applied external voltage in HiPIMS is also excluded for the simple reason that it has the wrong polarity.

Instead, it is here proposed that the cause of the sideways deflection of the ions is that the azimuthal current density J_ϕ above the race track exerts a volume force on the ions tangentially outwards as illustrated in Figure 1b, in accordance with what was stated in the introduction about radial ion transport related to anomalous transport. This force is proportional to the current density and the transverse resistivity, $\mathbf{F}_{i\phi} = -\eta_\perp en_e \mathbf{J}_\phi$. The strong deflection in the HiPIMS mode can be understood by the density-normalized resistivity, η_\perp ,

being typically an order of magnitude higher than in dcMS, leading to greater force transferred to the ions from the electrons. In order to see why there is an increase in resistivity, it is necessary to look into anomalous transport in more detail.

The macroscopic transverse resistivity given by the average over the azimuthally traveling wave structure can be rewritten as $\eta_{\perp} = \langle n_e E_{\phi} \rangle / J_{\phi} \langle n_e \rangle$ [20]. The effective momentum transfer time, often called the effective electron collision time, τ_c , is related to the resistivity through

$$\eta_{\perp} = \frac{m_e}{\tau_c e^2 n_e} = \frac{B}{\omega_{ge} \tau_c e n_e}, \quad (1)$$

where the electron angular gyro frequency, $\omega_{ge} = eB / m_e$. The product $\omega_{ge} \tau_c$ can, in the bulk plasma of magnetrons, where the current is carried mainly by the electrons, be directly obtained from a macroscopic measurement of the current density ratio as $\omega_{ge} \tau_c = J_{\phi} / J_D$ [5], where J_D is the discharge current density. In the case where the current is driven by an electric field, this follows directly from the ratio between the Hall and Pedersen conductivities [25], σ_H and σ_P respectively, and does not require $\omega_{ge} \tau_c \gg 1$ as sometimes stated:

$$\frac{J_{\phi}}{J_D} = \frac{E \sigma_H}{E \sigma_P} = \frac{E \cdot \frac{en_e}{B} \cdot \frac{\omega_{ge}^2 \tau_c^2}{1 + \omega_{ge}^2 \tau_c^2}}{E \cdot \frac{en_e}{B} \cdot \frac{\omega_{ge} \tau_c}{1 + \omega_{ge}^2 \tau_c^2}} = \omega_{ge} \tau_c. \quad (2)$$

In dcMS, measurements of J_{ϕ} / J_D give typical values in the range $8 < \omega_{ge} \tau_c < 30$ [26, 27], which is often referred to as the Bohm regime. Note that for the upper limit reference 26 proposes the value $\omega_{ge} \tau_c = 16$, but we find that it better fits $\omega_{ge} \tau_c = 30$. In HiPIMS and mid-frequency pulsed magnetrons, recent measurements [14, 15, 28] agree on a value close to $\omega_{ge} \tau_c = 2$. This means that the ratio of azimuthal current density to the discharge current density (or equivalently $\omega_{ge} \tau_c$), being roughly one order of magnitude lower compared to dcMS discharges, increases the transverse resistivity and thereby the tangential force on the ions.

For a numerical estimate of the ion acceleration due to the increased azimuthal force, quantities at the location of the maximum \mathbf{J}_ϕ current density, which is at $z = 0.01$ m above the race track, are taken. At the time of discharge current maximum, the following values are used (scaled from a study by Bohlmark *et al.* [14], as discussed by Lundin *et al.* [15]) : $B = 0.03$ T, $n_e = n_i = 10^{19}$ m⁻³, $J_\phi = 20 \times 10^3$ Am⁻², and $\eta_\perp = B / (\omega_{ge} \tau_c e n_e) = 0.01$ Ω m . The average azimuthal force per ion $\langle \mathbf{F}_{i\phi} \rangle / n_i = -\eta_\perp e n_i \mathbf{J}_\phi / n_i$, is with these values 3×10^{-17} N/ion. Ions above the race track will be subject to this force over a distance of typically $l = 0.05$ m (see Figure 1) and gain an average energy of $\langle \Delta W_{i\phi} \rangle = F \cdot l / e \approx 10$ eV . The sideways velocity gain, added to a predominantly vertical velocity (*i.e.* in the z direction) corresponding to about 5 eV from the sputtering process, is of the right order to give the observed deflection to the sides. Also, it gives a total average energy $\langle W_i \rangle \approx 15$ eV , in good agreement with the average ion energy of 18 eV in Figure 5. The spread in ion energy around the average is the expected result of different phase matching between individual ions and the wave structure as well as collisions. It can separately be checked if the highest ion energies of Figure 5 can result from the proposed acceleration mechanism. Ions that are accelerated azimuthally by the wave structure can reach at most the wave phase velocity $v_{phase,\phi}$. Since the waves are driven by the azimuthal electron drift $u_{e\phi}$ relative to the much slower moving ions, the situation is the following: $u_{i\phi,max} \leq u_{phase,\phi} \leq u_{e\phi}$. The range of $u_{e\phi}$ from 1.3×10^4 m s⁻¹ (at $z = 0.01$ m) to 5×10^4 m s⁻¹ (at $z = 0.04$ m) in the HiPIMS setup corresponds to a range in $W_{i,max} = m_i u_{e\phi}^2 / 2$ from 40 to about 600 eV , consistent with the measured highest ion energies in Figure 5 taking into consideration that the maximum detection energy is 100 eV. It is important to understand that the wave phase speed is a theoretical upper limit. The ions can probably not reach the full phase speed because of the limitations in spatial extent of the region where there is strong wave activity (*i.e.* in the torus-shaped plasma close to the race track region).

Last, the azimuthal kick of the ions as observed from the race track was verified in Figure 7, which is consistent of the picture of ions tangentially leaving the race track region

in the opposite direction of \mathbf{J}_ϕ as shown in Figure 1b. It can be also be seen that there is a small fraction of ions with $E_i > 20$ eV being measured by the mass spectrometer placed at position S_2 , contrary to what is expected if the ions were accelerated by the transport mechanism described. One possibility would be that the high-energy accelerated ions leaving the race track region undergo a collision as depicted in Figure 1b (the mean free path for these pressures is estimated to less than 0.1 m), which would change the direction enough, as well as lower the ion energy, so as to produce this type of distribution. On the other hand, the minimum in energy found around 5 eV on the HiPIMS curve of Figure 6, but not detected for dcMS, cannot be explained by azimuthal acceleration since the minimum looks identical when examining the distributions from both sides of the race track in Figure 7. The energy spectrum in this range is therefore probably determined by some other mechanism.

Conclusions

It is found that a substantial fraction of sputtered material is accelerated and transported radially away from the cathode and lost to the walls in HiPIMS discharges. This can help in understanding the decreased deposition rate measured for HiPIMS. The mechanisms for this radial acceleration of the target ions is believed to be due to a type of modified ion transport resulting from anomalous electron transport, previously reported in several pulsed magnetron experiments. In a series of time-averaged ion energy measurements, the Ti^+ energy distributions were recorded, which confirmed theoretical estimations on this type of transport regarding energy and direction.

Acknowledgements

This work was partly supported by the European Commission within the 6th framework (integrated project: InnovaTiAl).

References

- [1] Mozgrin D V, Fetisov I K and Khodachenko G V 1995 *Plasma Phys. Rep.* **21** 400
- [2] Kouznetsov V, Macák K, Schneider J M, Helmersson U and Petrov I 1999 *Surf. Coat. Technol.* **122** 290
- [3] Macák K, Kouznetsov V, Schneider J M, Helmersson U and Petrov I 2000 *J. Vac. Sci. Technol. A* **18** 1533
- [4] Gudmundsson J T, Alami J and Helmersson U 2002 *Surf. Coat. Technol.* **161** 249
- [5] Rossnagel S M and Kaufman H R 1986 *J. Vac. Sci. Technol. A* **4** 1822
- [6] Helmersson U, Lattemann M, Bohlmark J, Ehiasarian A P and Gudmundsson J T 2006 *Thin Solid Films* **513** 1
- [7] Alami J, Persson P O Å, Music D, Gudmundsson J T, Bohlmark J and Helmersson U 2005 *J. Vac. Sci. Technol. A* **23** 278
- [8] Christie D J 2005 *J. Vac. Sci. Technol. A* **23** 330
- [9] Helmersson U, Lattemann M, Alami J, Bohlmark J, Ehiasarian A P and Gudmundsson J T 2005 *Proceedings of the 48th Annual Technical Conference of the Society of Vacuum Coaters* (Denver, CO, USA) p 458
- [10] Konstantinidis S, Dauchot J P, Ganciu M and Hecq M 2006 *Appl. Phys. Lett.* **88** 021501
- [11] Bugaev S P, Koval N N, Sochugov N S and Zakharov A N 1996 *Proceedings of the XVIIth International Symposium on Discharges and Electrical Insulation in Vacuum* (Berkeley, CA, USA) p 1074
- [12] Bohlmark J, Östbye M, Lattemann M, Ljungcrantz H, Rosell T and Helmersson U 2006 *Thin Solid Films* **515** 1928
- [13] Emmerlich J, Mráz S, Snyders R, Jiang K and Schneider J M *in press* 2007 *Vacuum*
doi:10.1016/j.vacuum.2007.10.011
- [14] Bohlmark J, Helmersson U, VanZeeland M, Axnäs I, Alami J and Brenning N 2004 *Plasma Sources Sci. Technol.* **13** 654

- [15] Lundin D, Helmersson U, Kirkpatrick S, Rohde S and Brenning N 2008 *Plasma Sources Sci. Technol.* **17** 025007
- [16] Brenning N, Hurtig T and Raadu M A 2005 *Phys. Plasmas* **12** 012309
- [17] Hsia J B, Chiu S M, Hsia M F, Chou R L and Wu C S 1979 *Phys. Fluids* **22** 1737
- [18] Machida S, Abe T and Terasawa T 1984 *Phys. Fluids* **27**, 1928
- [19] Hurtig T, Brenning N and Raadu M A 2005 *Phys. Plasmas* **12** 012308
- [20] Hurtig T, Brenning N and Raadu M A 2004 *Phys. Plasmas* **11** 33
- [21] Bohlmark J, Lattemann M, Gudmundsson J T, Ehasarian A P, Aranda Gonzalvo Y, Brenning N and Helmersson U 2006 *Thin Solid Films* **515** 1522
- [22] Aranda Gonzalvo Y Hiden Analytical Ltd. *private communication*
- [23] Ehasarian A P, Hovsepian P Eh, Hultman L and Helmersson U 2004 *Thin Solid Films* **457** 270
- [24] Kadlec S 2007 *Plasma Proc. Polym.* **4** S419
- [25] Fälthammar C-G 1991 *Space Physics* (Stockholm) Department of Plasma Physics, Royal Institute of Technology p 50
- [26] Rossnagel S M and Kaufman H R 1987 *J. Vac. Sci. Technol. A* **5** 2276
- [27] Bradley J W, Thompson S and Aranda Gonzalvo Y 2001 *Plasma Sources Sci. Technol.* **10** 490
- [28] Vetushka A and Bradley J W 2007 *J. Phys. D* **40** 2037